Coplanar corporate feed effects in microstrip patch array design

P.S. Hall, MEng, PhD, CEng, MIEE
C.M. Hall, BSc, PhD

Indexing terms: Antennas (microstrip), Antennas (stripline), Microstrip and stripline

Abstract: The use of coplanar corporate feeds for microstrip patch arrays leads to constructional simplicity, but also to performance degradations due to feed radiation, in addition to limitations due to feed resistive loss, surface waves, mutual coupling and tolerances. These effects are quantified, and this allows specification of array performance limitations in addition to the recommendation of the use of smooth feed discontinuities, high line impedance, and thin substrates. Improvements due to the use of alternate feed geometries, such as sequentially rotated feeding and subarraying, are also quantified and are shown to be substantial.

1 Introduction

Microstrip array antennas are now being actively considered for applications, such as satellite communication systems [1, 2], where their thin profile and light weight are important considerations. The array thickness, weight, and cost can be optimised by the use of a corporate feed structure etched on the same surface as the patch array, as shown in Fig. 1. However, feed resistive losses and radiation lead to gain and radiation pattern limitations, making feed effects a key issue in the design of such arrays. Experimental investigations [3] have highlighted these problems, although to the authors knowledge no detailed results allowing design optimisation have been published. In this paper these effects, together with other design perturbations such as surface waves, mutual coupling, and tolerances, are quantified to allow a more complete understanding of performance limitations and of methods [4] by which these limitations can be improved upon with a view to their implementation in computer-aided design (CAD).

2 Corporate feed loss mechanisms

Losses in microstrip corporate feeds are due to copper and to dielectric losses in straight lengths compounded with radiation and surface-wave losses from the overall structure, the complete quantification of which requires detailed knowledge of the current distribution on the feed network. First order estimates have been obtained by isolating and assessing these various components and in following Sections these estimates are used to deduce their effects on efficiency and on the array radiation pattern.

Paper 5965H (E11) first received 17th July and in revised form 22nd December 1987

The authors are with the School of Electrical Engineering and Science, Royal Military College of Science, Shrivenham, Wiltshire SN6 8LA, United Kingdom

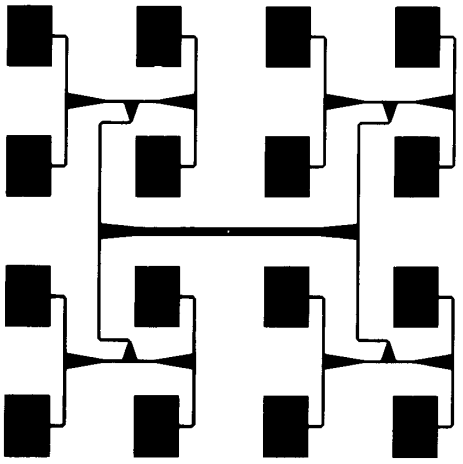

Fig. 1 *Silhouette of corporately fed patch array for linear polarisation with uniform aperture distribution*
$\varepsilon_r = 2.32$; $h = 1.59$ mm; $h/\lambda_0 = 0.06$; frequency = 12.0 GHz; $d/\lambda_0 = 0.7$

2.1 Line loss

I^2R and dielectric losses have been estimated by many authors. Based on comparative studies of applicability and accuracy we recommend estimates of attenuation coefficient due to dielectric loss α_d and copper loss α_c by Pucel [5], based on an analysis of the effective dielectric constant ε_e and the microstrip wavelength λ_m by Wheeler [6] and Kirschning *et al.* [7]. α_c must then be corrected for roughness effects [8] to give α_{cr}. Fig. 2*a* shows total line loss $(\alpha_d + \alpha_{cr})$ for two types of substrate. It can be seen that line loss increases with dielectric constant and line impedance, and decreases with increasing substrate thickness.

2.2 Radiation loss

Estimations of radiation from microstrip discontinuities are based on analyses of equivalent electric and polarisation currents [9, 10]. The ratio of power radiated to power incident on the discontinuity is given by Reference 9 as

$$\frac{P_r}{P_{inc}} = \frac{60(\beta h)^2}{Z} \cdot F \tag{1}$$

where $\beta = 2\pi/\lambda_0$, h is the substrate thickness, and Z is the impedance of the input line. For the coaxial-to-microstrip transition of Fig. 1, F is found by combining

that owing to a conventional transition [9] and that owing to a continuous line, to give

$$F = \frac{1}{4}\left\{3 - \frac{1}{\varepsilon_e} - \left(3 + \frac{1}{\varepsilon_e}\right) \cdot \frac{\varepsilon_e - 1}{2\sqrt{\varepsilon_e}} \cdot \frac{\ln \sqrt{(\varepsilon_e)} + 1}{\sqrt{(\varepsilon_e)} - 1}\right\} \quad (2)$$

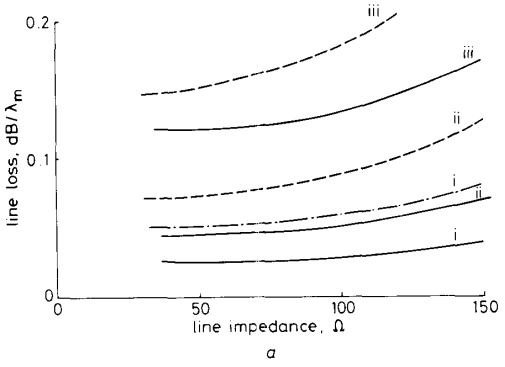

a

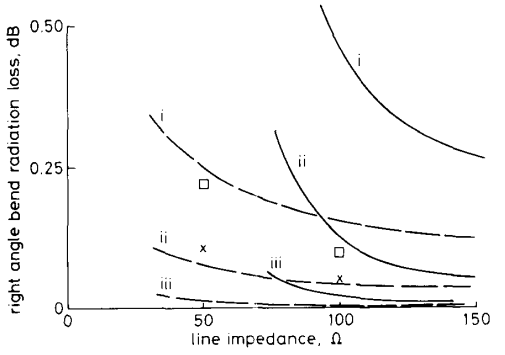

b

Fig. 2 *Calculated microstrip line loss and discontinuity radiation loss*
a Line loss $\alpha_d + \alpha_{cr}$
b Right angle bend radiation loss P_r/P_{inc}
——— $\varepsilon_r = 1.0$
- - - - $\varepsilon_r = 2.32$
i $h/\lambda_0 = 0.06$
ii $h/\lambda_0 = 0.03$
iii $h/\lambda_0 = 0.01$

Smooth 90° bend, $\varepsilon_r = 2.32$; $h/\lambda_0 = 0.06$; bend radius □ $\rho = 0.2\lambda_0$; × $\rho = 0.4\lambda_0$

where ε_e is the effective dielectric constant of the microstrip line. Radiation loss decreases with decreasing substrate thickness and increasing dielectric constant, being less than 0.1 dB for $h/\lambda_0 = 0.03$ with $\varepsilon_r = 1.0$ and for $h/\lambda_0 = 0.06$ with $\varepsilon_r = 2.32$. For the right angle bend [9], whether mitred or not, F is given by

$$F = \frac{\varepsilon_e + 1}{\sqrt{\varepsilon_e}} \ln \frac{\sqrt{(\varepsilon_e)} + 1}{\sqrt{(\varepsilon_e)} - 1} - \frac{2\varepsilon_e}{\sqrt{2\varepsilon_e - 1}} \ln \frac{\sqrt{2(\varepsilon_e - 1)} + 1}{\sqrt{2(\varepsilon_e - 1)} - 1} \quad (3)$$

while for the T junction [11]

$$F = \frac{(3\varepsilon_e + 1)^2}{8\varepsilon_e^{3/2}} \ln \frac{\sqrt{(\varepsilon_e)} + 1}{\sqrt{(\varepsilon_e)} - 1} - \frac{\varepsilon_e}{2\varepsilon_e - 1} \times \ln \frac{\varepsilon_e + \sqrt{(2\varepsilon_e - 1)}}{\varepsilon_e - \sqrt{(2\varepsilon_e - 1)}} - \frac{\varepsilon_e + 1}{4\varepsilon_e} \quad (4)$$

Fig. 2*b* shows radiation loss for the right angle bend. Similar values are obtained for the T junction. For a smooth-radiused bend a constant equivalent magnetic current $\boldsymbol{M}_e$ located at the microstrip line centre is assumed, where $\boldsymbol{M}_e$ is given by [12],

$$\boldsymbol{M}_e = \hat{\boldsymbol{\phi}} V kw \left\{\frac{1}{k\rho} + j \cos\phi \sin\theta\right\} \exp(-j\beta\phi\rho) \quad (5)$$

where V is the line voltage, ρ is the line radius, $k = 2\pi/\lambda_m$ and (θ, ϕ) are far-field spherical coordinates. Integration of the radiation vector due to this current $\boldsymbol{M}_e$ over the bend allows the radiated power to be obtained, and from this the radiation loss as shown in Fig. 2*b*. It is seen that considerable reduction occurs for increasing bend radius. Variational analysis of the radiation from a quarter-wavelength matching section [13] from 50 to 100 Ω shows that radiation loss is typically below 0.02 dB for low dielectric constant substrates. These results, therefore, indicate that the most significant radiation loss occurs in T junctions and right angle bends. Reductions can be obtained by the use of thin high dielectric constant substrates, high line impedances, and radiused bends.

3 Radiation pattern effects

3.1 Feed radiation

The effect of feed radiation on the array patterns has been analysed using a source distribution of magnetic currents [14, 15]. The patch-source distribution $\boldsymbol{M}$ is a continuous current around the patch periphery, whose value is determined from a patch cavity model including the fundamental and higher-order modes. The feed-source distribution $\boldsymbol{M}_q$ is made up of discrete Hertzian currents located at the feed discontinuities. Thus the radiated field $\boldsymbol{E}_{rad}$ is given by

$$\boldsymbol{E}_{rad} = jhk[\hat{\boldsymbol{R}} \times \int_c \boldsymbol{M} \exp(jk_0 r \cos\psi)\, dc] + jhK \sum_{q=1}^{Q} M_q \exp(jk_0 r_q \cos\psi_q)\{\sin(\phi - \gamma_q)\hat{\boldsymbol{\theta}} - \cos\theta \cos(\phi - \gamma_q)\hat{\boldsymbol{\phi}}\} \quad (6)$$

where $K = \exp(-jk_0 R)/\lambda_0 R$, $\boldsymbol{R}$ is a unit vector in the far field direction, and r, ψ, (r_q, ψ_q) define the magnetic-current source position [14]. γ_q defines the Hertzian current orientation [14]. The discontinuity magnetic current value M_q is given by

$$M_q = I_q Z_0 \sqrt{\left(\frac{3}{2} F_q\right)} \quad (7)$$

where Z_0 is the free space impedance: F_q is given by eqns. 2, 3 or 4.

The current on the qth discontinuity I_q is given by

$$I_q = \left\{\frac{P_{in}\lambda_m}{Z_q \alpha q l_q}\right\}^{1/2} \exp\{-j(k_m l_q + e_q)\} \quad (8)$$

P_{in} is the array input power; Z_q is the line impedance at the qth transition; $\alpha = \alpha_d + \alpha_{cr}$, l_q is the line length between the q and $(q-1)$th transitions; k_m is the microstrip line wavenumber; e_q is the reference plane extension for the qth discontinuity [8]. The discontinuity numbering is arranged so that q is the number of input lines to a particular stage of power division in the corporate feed. $q = 1$ for the coax to microstrip transition and for subsequent stages $q = 2, 4, 8$, etc.

Fig. 3 shows computed results compared to measurements for an 8 × 8 element array of the form of Fig. 1. Agreement is good down to a level of −15 dB but below this the analytical approximations, and in particular the

difficulties in accurate calculation of the relative phase of the feed contributions, lead to errors. Examination of the measured patterns also indicates that the high sensitivity

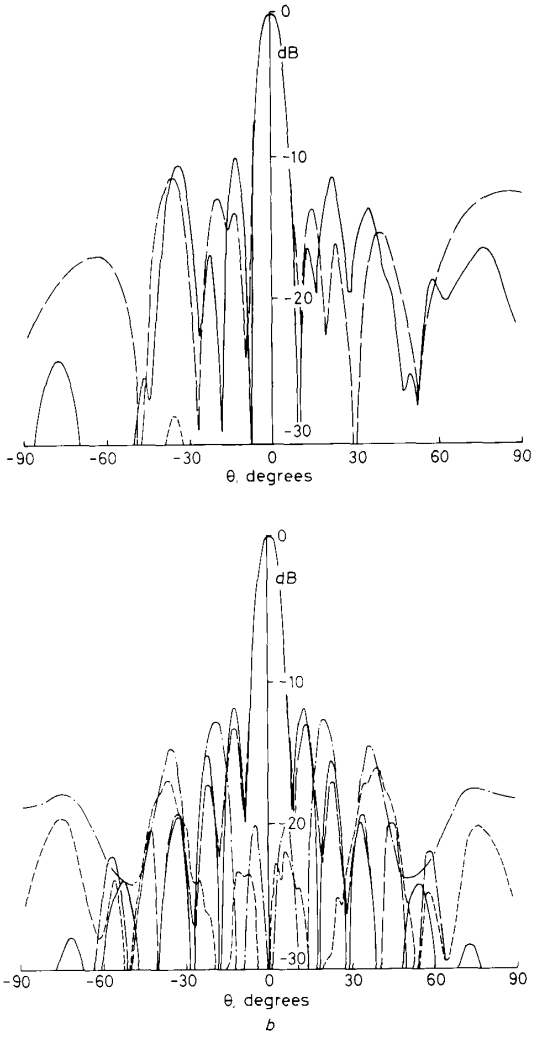

Fig. 3 *Radiation patterns of 8 × 8 element array as Fig. 1*
a E-plane
b H-plane
$h/\lambda_0 = 0.06$; $\varepsilon_r = 2.32$; frequency = 12 GHz
——— measured } copolarised
— — theoretical }
- - - - measured } crosspolarised
—·— theoretical }

of the feed-radiation pattern to frequency may reduce the overall array bandwidth, if this is determined by pattern quality in addition to input voltage standing-wave ratio (VSWR). Fig. 4 shows the computed patterns of a 16 × 16 element array. Here the pattern of the feed alone, that is with the patch radiation supressed, is compared to the envelope of the sidelobe pattern of the patches alone. It can be seen that feed sidelobes are in some cases of the order of 10 dB higher than patch radiation. A symmetrical grating structure is noted in the *H*-plane of the feed radiation.

The relative contributions of the various feed discontinuities can be estimated by multiplying the radiation levels given in Section 2 by a gain associated with the array effect for the particular discontinuity considered. Thus the discontinuity gain, G, is given by

$$G = \frac{Z_q I_q^2}{P_{in}} \cdot \frac{P_r}{P_{inc}} \cdot A_d g_d \tag{9}$$

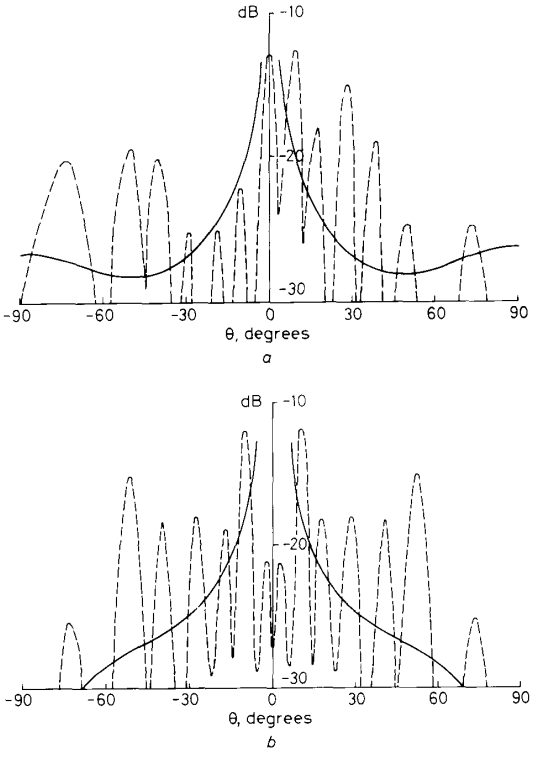

Fig. 4 *Calculated radiation pattern of 16 × 16 element array as Fig. 1*
——— sidelobe envelope of patches
a E-plane
- - - - copolarised feed pattern
b H-plane
- - - - crosspolarised feed pattern

$Z_q I_q^2 / P_{in}$ is the ratio of power incident on the discontinuity to the array input power deduced from eqn. 8; P_r/P_{inc} is the fraction of incident power radiated by the discontinuity as deduced from eqn. 1; A_d is the discontinuity array factor involving the total number of each type of discontinuity and their spacing; g_d is the gain of a Hertzian magnetic current source. For a 16 × 16 element array the following values are found. For the *T*-junctions next to the patches $G = 5.0$ dBi, which is about 23 dB down on the peak array gain; for the input connector $G = -8.0$ dBi, about 36 dB down. G for the other discontinuities is between these values, and decreases monotonically towards the centre of the array. This result indicates that the discontinuities nearest the patches have the greatest effect on the array radiation pattern.

3.2 Substrate surface wave scattering

This is characterised by S_L, the ratio of surface-wave generation to radiation [16] representing a peak of likely sidelobe perturbation, and by $S_A = S_L/G_A$ where G_A is the array gain which represents the mean sidelobe level. S_L is approximately −13 dB, −18 dB and −22 dB for $h/\lambda_0 = 0.06$, 0.03 and 0.01, respectively, with $\varepsilon_r = 2.32$. The mean sidelobe level S_A will be significantly lower than this and will decrease with increasing array size. This trend agrees with results given by analysis of finite microstrip arrays using the moments method [17],

although actual surface-waves levels are somewhat lower here.

3.3 Mutual coupling effects

The effect of mutual coupling has been calculated by incorporating mutual admittance values given by the magnetic-current method [18] into a forced excitation model of the feed-array interaction. Hence

$$[V] = [Z][I] \tag{10}$$

where $[V]$ is the element voltage matrix, $[Z] = [Y]^{-1}$ is the array self and mutual impedances matrix, and $[I]$ is the constant current excitation matrix. Table 1 shows the

Table 1: Computed peak increase in sidelobe level in linear patch array due to mutual coupling

Number of elements	Peak increase in sidelobe level, dB	
	E-plane	*H*-plane
8	2.6	0.5
16	4.0	0.5

$\varepsilon_r = 2.32$; $h/\lambda_0 = 0.06$; $d/\lambda_0 = 0.7$

peak increase in the sidelobe level for linear patch arrays with uniform excitations. Increases in the *E*-plane are considerably higher than in the *H*-plane. Such increases may well account for the higher measured sidelobes noted in Fig. 3. For tapered aperture distributions larger increases are only noted in the smaller arrays. Mutual coupling effects also decrease with decreasing dielectric constant and substrate thickness.

3.4 Design and production tolerances

The maximum rise in sidelobe level L_{max} due to tolerance effects is given [19] by

$$L_{max} = 10 \log_{10}\{1 + 10^{s/10}K(\sigma_1^2 + 2\sigma_2^2 + 2f^2)\} \tag{11}$$

s is the design sidelobe level (in dB); K is a constant relating to array size; σ_1^2 and σ_2^2 are the variances of positional and angular element errors; f relates to errors in element excitation. Estimates have been based on experience of production tolerances achieved at RMCS, manufacturers quoted material tolerances in height and dielectric constant, and previous corporate feed analysis [20]. Table 2 gives typical values of L_{max}. It can be seen

Table 2: Maximum rise in sidelobe level L_{max} due to design and production tolerances in a two dimensional array

Design sidelobe level *D*, dB	L_{max}, dB	
	$N = 16$	$N = 64$
13 (uniform distribution)	0.04	0.00
20	0.20	0.04
30	2.10	0.42

Array size = N elements; $\varepsilon_e = 2.32$; $h/\lambda_0 = 0.06$; $d/\lambda_0 = 0.7$; $\sigma_1^2 = 0.0025$; $\sigma_2^2 = 0.01$; $f^2 = 0.09$

from the caption that excitation error f^2 dominate, owing primarily to material and production tolerance effects in the feed network. However, overall sidelobe increases are well below those due to feed radiation. Excitation errors and hence sidelobe errors will increase with increasing substrate dielectric constant owing to the increased electrical line lengths involved for a given array size. The effect of substrate height is less clear.

4 Array gain and efficiency

Gain reduction in microstrip patch arrays is due to losses in the feed line and patches and to losses due to feed radiation, surface wave generation, mutual coupling, and design and manufacturing tolerance errors. The total feed loss L_f in a two dimensional patch array is given by Reference 21 as follows:

$$L_f \approx \frac{\alpha d}{\lambda_m}(\sqrt{(N)} - 1) + n_t l_t + n_b l_b + l_c \tag{12}$$

$\alpha = \alpha_d + \alpha_{cr}$; N is the total number of elements; d is the element spacing; l_t, l_b and l_c are the radiation losses in dB of a T-junction, bend and coax to microstrip transition, respectively, deduced from eqns. 4, 3 and 2, respectively, with eqn. 1. n_t is the number of T-junctions; n_b is the number of bends. For the configuration of Fig. 1 $n_b = 3$. Gain loss L_t due to array design and production tolerances is given by Reference 22 as follows:

$$L_t = 1 + \sigma^2 \tag{13}$$

$\sigma^2 = \sigma_1^2 + \sigma_2^2 + f^2$ is the total error variance, eqn. 11; for values given in Table 2 $L_t = 0.4$ dB and is independent of array size; gain loss due to mutual coupling is given by the analysis of Section 3.3 and, assuming that the feed is matched to the active impedance of the array central element, is less than 0.1 dB for arrays of less than 16 × 16 elements. Patch resistive and surface wave losses are given by Reference 23.

Fig. 5 shows that overall array loss increases with increasing substrate height, decreasing dielectric constant and feed impedance. For arrays smaller than 16 × 16 elements total feed radiation is greater than resistive losses. Above this the high line losses make such arrays impractical. The rapid increase in loss with size gives rise to a maximum gain value for coplaner fed arrays which is illustrated in Fig. 6. A peak gain of about 35 dB is indicated, corresponding to an efficiency of about 10%.

5 Design implications and array optimisation

5.1 Substrate choice

Table 3 summarises the deductions relating to substrate

Table 3: Optimum substrate parameter choice for array performance requirements

Requirement	Dielectric constant	Substrate thickness
1 Low feed radiation	high	thin
2 Low surface waves	low	thin
3 Good tolerance control	low	thin
4 Low mutual coupling	low	thin
5 Low array losses	high	thin
6 Wide bandwidth	low	thick

For substrates $1 < \varepsilon_r < 2.5$; $0.01 < h/\lambda_0 < 0.1$

choice. The overall requirements are contradictory, with low dielectric constant leading to wider bandwidths but in particular increased array losses and thin substrates leading to all round array benefits at the cost of narrow bandwidth. These trade-offs are further illustrated in Table 4, where the effect of substrate thickness on array efficiency and bandwidth is given. It can be seen that substantial increases in efficiency are obtained by use of thin substrates but at the expense of patch bandwidth. Decreases in substrate thickness are accompanied by reduced pattern perturbation due to feed radiation as shown in Fig. 7, and the perturbation may be reduced to

a relative level of −25 dB if the thickness is decreased to the order of $h/\lambda_0 = 0.01$. This perturbation level is comparable to surface-wave levels, and is less than those due to mutual coupling. The bandwidth constraint of thin substrates can be overcome to some extent by the use of electromagnetic coupling to overlaid patches [24] or the use of a separate feed layer, although the penalty of increased constructional complexity is incurred.

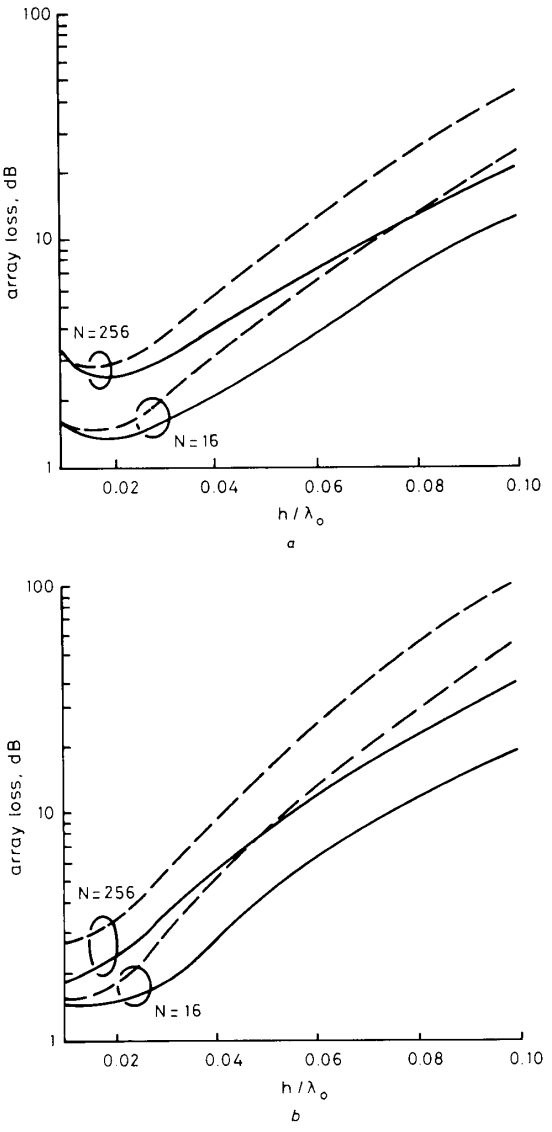

Fig. 5 *Overall loss of corporately fed microstrip array*
a $\varepsilon_r = 2.32$
b $\varepsilon_r = 1.06$
Assumes feed form of Fig. 1; element spacing = $0.8\lambda_0$
——— feed impedance = 100 Ω
– – – – feed impedance = 50 Ω

Table 4: Computed efficiency and bandwidth of 16 × 16 patch array

Feed type	Feed height, h/λ_0	Efficiency, %	Patch bandwidth, % (to −10 dB return loss points)
As Fig. 1	0.06	39	5
As Fig. 1 but with smoothed bends and splitters ($\rho/\lambda_0 = 0.5$)	0.03	57	2
	0.01	64	1
As Fig. 8	0.06	55	5

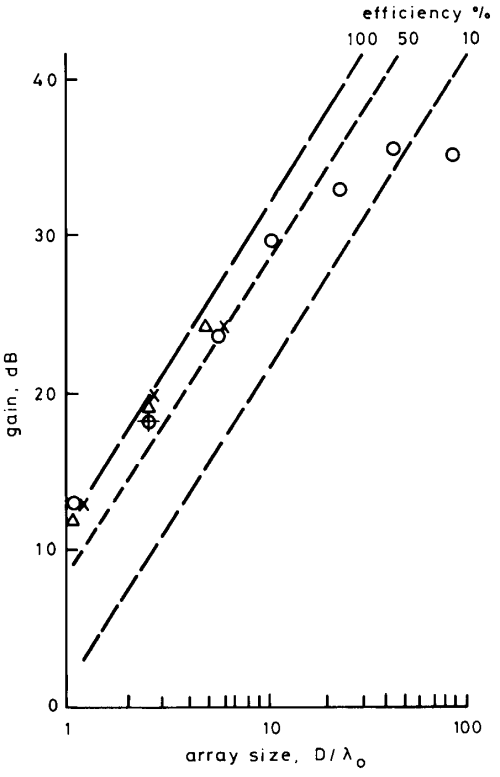

Fig. 6 *Array gain*
○ estimates based on results of Fig. 5
× measured, feed impedance 120 Ω, as Fig. 1
△ measured, Reference 3, feed impedance 200 Ω; $h/\lambda_0 = 0.06$; $\varepsilon_r = 2.1$
\+ measured, Reference 21, feed impedance = 100 Ω; $h/\lambda_0 = 0.0036$; $\varepsilon_r = 2.32$

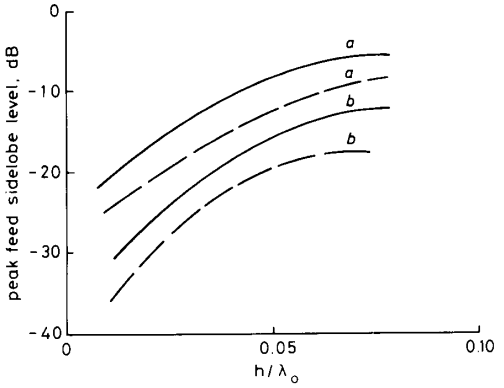

Fig. 7 *Calculated peak sidelobe level of feed radiation of 4 × 4 element array*
——— $\varepsilon_r = 1.06$
— — $\varepsilon_r = 2.32$
a Array as Fig. 1
b Array as Fig. 8

5.2 Feed geometry

The use of smooth bends to reduce feed radiation has been noted in Table 4, and is cited as an example of optimisation of the feed geometry. A further example is in the

use of sparse arrays with spherical dielectric overlays [25], where at the expense of more constructional complexity the number of feed discontinuities is significantly reduced, thus decreasing feed loss and pattern disturbance. However, an example combining optimised performance with manufacturing simplicity is that of sequentially rotated feeding for circularly polarised arrays [26]. This technique involves providing to the mth array element both a physical rotation and a feeding phase shift Φ_m given by

$$\Phi_m = \frac{2\pi(m-1)}{N} \quad 1 < m < N \tag{14}$$

where N is the array size. N may constitute the complete array or be a sub-array of a larger one. The principle has been applied to $N = 2$ arrays [1] and here to $N = 2 \times 2$ arrays [4]. These subarrays are used to form the complete array by applying sequential rotation to their feeding, as shown in Fig. 8. The overall geometry has less

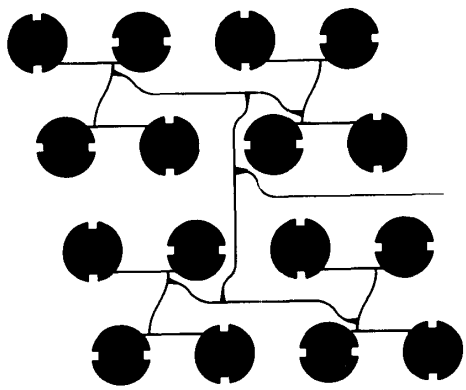

Fig. 8 *Silhouette of disc array for circular polarisation using sequentially rotated feeding*

feed discontinuities than the conventional feed of Fig. 1. Additionally, the feeding phase shifts cause radiation from adjacent T-junction pairs to be co-phased, and hence add into the main beam, reducing gain loss and sidelobe levels. The slanted patch configuration is used to reduce far out grating lobes in the 45° planes, owing to feed discontinuities with spacings greater than the free space wavelength.

Table 4 shows the increase in efficiency to be expected from this method, deduced from first-order consideration of the grating lobe structure of each pair of feed discontinuities. Figs. 9*a* and 9*b* show the computed radiation patterns of 16 × 16 element versions of the arrays of Fig. 8 and Fig. 1, respectively. Significant reduction of the overall sidelobe levels is obtained, particularly at wide angles. Fig. 7 shows that peak feed sidelobe levels for 4 × 4 element arrays fall by up to 10 dB for equivalent substrate thickness. Ultimately, the realisable sidelode levels for practical arrays using this feed method will of course depend on the relative levels of feed radiation, surface-wave, mutual coupling, and tolerance effects; however, significant reduction is expected for small arrays where feed radiation effects dominate.

5.3 Subarraying

Improved radiation pattern control and increased efficiency can be obtained by splitting the array into subarray sections, as indicated in the inset to Fig. 10. Each subarray is then fed by a low-loss corporate feed located behind the microstrip groundplane (as for example in Reference 1). Fig. 10 quantifies the advantage of subarraying within a 32 × 32 element patch array. It can be

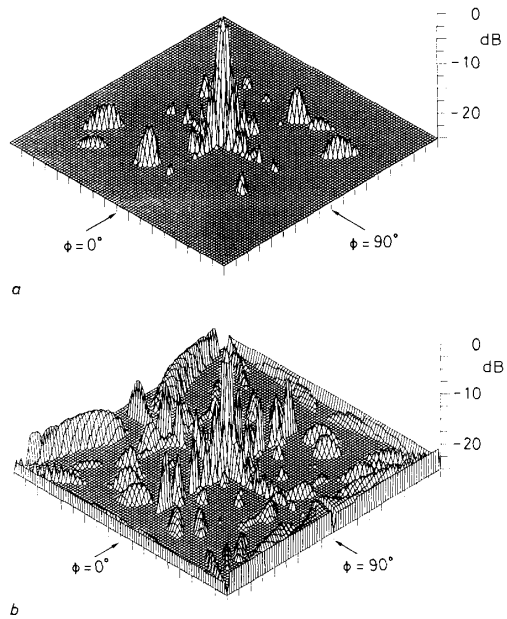

Fig. 9 *Computed radiation patterns of 16 × 16 patch array*
a Array as Fig. 8
b Array as Fig. 1
level shown is peak radiation whether co- or crosspolarised

seen from Fig. 10*a* that significant suppression of array sidelobes occurs for subarray sizes of 8 × 8 elements and less, particularly for the conventional corporate feed (Fig. 1), although sidelobe levels of the order of −25 dB are still expected. The use of sequential rotation for circular polarisation (Fig. 8), is seen to be advantageous for larger subarray sizes. The efficiency (Fig. 10*b*), for subarray size less than 4 × 4 elements, is determined primarily by feed-radiation loss and patch-dissipative and surface-wave losses. The advantages of subarray construction become greater for larger array size and indeed may be forced on designers by limited commercially available substrate sizes.

6 Conclusions

The use of coplanar microstrip feed networks for microstrip patch arrays allows simple construction, but incurs both gain loss and degradation in sidelobe and cross polarisation due to resistive loss and feed radiation. In comparison to these effects substrate surface wave and tolerance problems are small, although mutual coupling can be significant. For example in an 8 × 8 elemnt array with uniform distribution and 5% bandwidth, less than 55% efficiency is achieved with a sidelobe level of −10 dB. These effects are minimised by the use of smooth feed discontinuities, high feed line impedance, and thin substrates with a dielectric constant between 2 and 3, although the substrate recommendation will compromise bandwidth. Electromagnetic coupling to overlaid patches, shielded feeds or sparse arrays with overlaid lenses will overcome the bandwidth problem at the expense of constructional simplicity. The use of sequentially-rotated circularly-polarised arrays maintains simplicity, while reducing peak sidelobes by up to 10 dB.

Subarrays fed by low-loss shielded feeds will further improve performance.

The use of patch arrays with coplanar feed networks will thus give poorer performance than arrays with fully-shielded feeds or other antenna types such as reflectors. However, some degree of perfomance optimisation is possible and this, together with their potential low cost and volume, makes them attractive for a wide variety of applications. In addition such arrays lend themselves readily to computer aided design and production, and the first order analytical expressions and performance trade offs given here are likely to be an important element in such techniques.

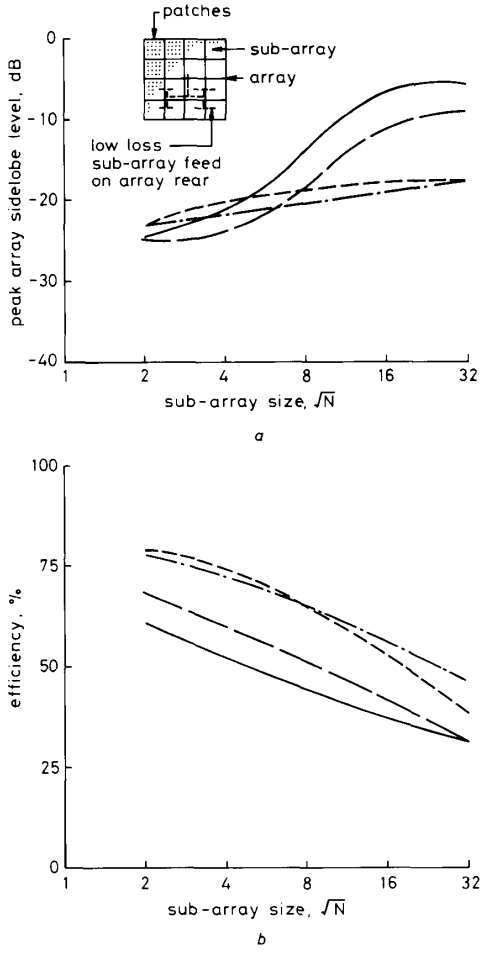

Fig. 10 *Performance of array of coplanar microstrip subarrays fed by low loss network*

a Peak array sidelobe level
b Array efficiency
Number of subarray elements = N; number of array elements = 32 × 32; inset shows example for $N = 16$ (i.e. subarray = 4 × 4 elements) microstrip coplanar feed within subarray; low loss (0.1 dB/λ_d, $\lambda_d = \lambda_0/\sqrt{2.5}$) feed connects subarrays
array of form of Fig. 1:
——— $\varepsilon_r = 1.06$
— — $\varepsilon_r = 2.32$
array of form of Fig. 8:
—·—· $\varepsilon_r = 1.06$
- - - - $\varepsilon_r = 2.32$

7 Acknowledgments

C.M. Hall was partly supported by the US Army, European Research Office. The authors would like to thank members of the Wolfson RF Engineering centre, RMCS, for useful discussions. The assistance of Mr L. Petterson of the Swedish Defence Research Institute, in the derivation of eqn. 2 is also acknowledged.

8 References

1 HANEISHI, M.: 'A circularly polarised SHF planar array composed of microstrip pairs elements', *Proc. ISAP 85*, Tokyo, Japan, August 1985, pp. 125–128
2 SHEEHAN, P.G., and FORREST, J.R.: 'Satellite-borne active phased array techniques for mobile communications' *IEE Proc. F, Commun., Radar & Signal Process.*, 1986, **133,** (4), pp. 339–344
3 ASHKENAZY, J., PERLMUTTER, P., and TREVES, D.: 'A modular approach for the design of microstrip array antennas', *IEEE Trans.*, 1983, **AP-31,** pp. 190–193
4 HALL, P.S.: 'Feed radiation effects in sequentially rotated microstrip patch arrays', *Electron. Lett.*, 1987, **123,** pp. 877–878
5 PUCEL, R.A., MASSE, D., and HARTWIG, C.P.: 'Losses in microstrip', *IEEE Trans.*, 1968, **MTT-16,** pp. 342–350 and p. 1064
6 WHEELER, H.A.: 'Transmission line properties of parallel strips separated by a dielectric sheet', *IEEE Trans.*, 1965, **MTT-13,** pp. 172–185
7 KIRSCHNING, M., and JANSEN, R.H.: 'Accurate model for effective dielectric constant of microstrip with validity up to millimetre-wave frequencies', *Electron. Lett.*, 1982, **18,** (6), pp. 272–273
8 HAMMERSTAD, E.O., and BEKKADAL, F.: 'Microstrip Handbook' ELAB report STF 44 A74169, University of Trondheim, Norwegian Institute of Technology
9 LEWIN, L.: 'Radiation from discontinuities in stripline', *IEE Proc. C*, 1960, **107,** pp. 163–170
10 HALL, P.S.: 'Microstrip linear array with polarisation control', *IEE Proc. H, Microwaves, Opt. & Antennas*, 1983, **130,** (3), pp. 215–224
11 LEWIN, L.: 'Spurious radiation from microstrip', *Proc. IEE*, 1978, **125,** (7), pp. 633–642
12 WOOD, C.: 'Curved microstrip lines as compact wideband circularly polarised antennas', *IEE J. Microwaves Opt. & Acoust.*, 1979, **3,** (1), pp. 5–13
13 HENDERSON, A., and JAMES, J.R.: 'Design of microstrip antenna feeds, Part 1: estimation of radiation loss and design implications', *IEE Proc. H, Microwaves, Opt. & Antennas*, 1981, **128,** (1), pp. 19–25
14 HALL, P.S., and JAMES, J.R.: 'Crosspolarisation behaviour of series-fed microstrip linear arrays', *IEE Proc. H, Microwaves, Antennas & Propag.*, 1983, **131,** (4), pp. 247–257
15 HALL, P.S., and PRIOR, C.J.: 'Microstrip array for reflector feed applications', 14th European Microwave Conference, Liege, Belgium, September 1984, pp. 631-636
16 JAMES, J.R., and HENDERSON, A.: 'High frequency behaviour of microstrip open-circuit terminations', *IEE J. Microwaves, Opt. & Acoust.*, 1979, **3,** pp. 205–211
17 POZAR, D.M.: 'Finite phased arrays of rectangular microstrip patches', *IEEE Trans.*, 1966, **AP-34,** pp. 658–665
18 PENARD, E., and DANIEL, J.P.: 'Mutual coupling between microstrip antennas', *Electron. Lett.*, 1982, **18,** pp. 605–607
19 ELLIOT, R.S.: 'Mechanical and electrical tolerances for two dimensional scanning arrays', *IRE Trans.*, 1958, **AP-6,** pp. 114–120
20 HALL, P.S., and JAMES, J.R.: 'Design of microstrip antenna feeds: Part 2', *IEE Proc. H, Microwaves, Opt. & Antennas*, 1981, **128,** (1), pp. 26–34
21 HALL, C.M.: 'Millimetre-wave microstrip antennas and hybrid types', PhD thesis, Royal Military College of Science, Shrivenham, February 1987
22 RUDGE, A.W., MILNE, K., OLVER, A.D., and KNIGHT, P.: 'Handbook of antenna design' (Peter Perigrinus, London, 1983) Vol 2, p. 76
23 JAMES, J.R., HENDERSON, A., and HALL, P.S.: 'Microstrip antenna performance is determined by substrate constraints', *Microwave Systems News*, 1982, **2,** pp. 73–84
24 HALL, P.S., and PRIOR, C.J.: 'Microwave feeds for prime focus fed reflector antennas, *IEE Proc. H, Microwaves, Antenna & Propag.*, 1987, **134,** (2), pp. 185–193
25 JAMES, J.R., HALL, C.M., and ANDRASIC, G.: 'Microstrip elements and arrays with spherical dielectric overlays', *IEE Proc. H, Microwaves, Antenna & Propag.*, 1986, **133,** (6), pp. 474–482
26 TESHIROGI, T., TANAKA, M., and CHUJO, W.: 'Wideband circularly polarised array with sequential rotation', Proc. ISAP, Tokyo, Japan, August 1985, pp. 117–120